Human Molecular Genetics, 2015, 1–14

doi: 10.1093/hmg/ddv187
Advance Access Publication Date: 22 May 2015
Original Article

ORIGINAL ARTICLE

Model mice for 15q11–13 duplication syndrome exhibit late-onset obesity and altered lipid metabolism

Rui Kishimoto[1,2,†], Kota Tamada[1,2,†], Xiaoxi Liu[1], Hiroko Okubo[1], Satoko Ise[3], Hisashi Ohta[3], Sandra Ruf[4], Jin Nakatani[5], Nobuoki Kohno[2], François Spitz[4] and Toru Takumi[1,2,6,*]

[1]RIKEN Brain Science Institute, Wako, Saitama 351-0198, Japan, [2]Graduate School of Biomedical Sciences, Hiroshima University, Minami, Hiroshima 734-8553, Japan, [3]Banyu Tsukuba Research Institute, Tsukuba, Ibaraki 300-2611, Japan, [4]Developmental Biology Unit, European Molecular Biology Laboratory, Heidelberg, Germany, [5]Molecular Neuroscience Research Center, Shiga University of Medical Science, Ohtsu, Shiga 520-2192, Japan and [6]JST, CREST, Tokyo, Japan

*To whom correspondence should be addressed at: RIKEN Brain Science Institute, 2-1 Hirosawa, Wako, Saitama 351-0198, Japan. Email: toru.takumi@riken.jp

Abstract

Copy number variations on human chromosome 15q11–q13 have been implicated in several neurodevelopmental disorders. A paternal loss or duplication of the Prader–Willi syndrome/Angelman syndrome (PWS/AS) region confers a risk of obesity, although the mechanism remains a mystery due to a lack of an animal model that accurately recreates the obesity phenotype. We performed detailed analyses of mice with duplication of PWS/AS locus (6 Mb) generated by chromosome engineering and found that animals with a paternal duplication of this region (*patDp/+*) show late-onset obesity, high sensitivity for high-fat diet, high levels of blood leptin and insulin without an increase in food intake. We show that prior to becoming obese, young *patDp/+* mice already had enlarged white adipocytes. Transcriptome analysis of adipose tissue revealed an up-regulation of *Secreted frizzled-related protein 5* (*Sfrp5*), known to promote adipogenesis. We additionally generated a new mouse model of paternal duplication focusing on a 3 Mb region (3 Mb *patDp/+*) within the PWS/AS locus. These mice recapitulate the obese phenotypes including expansion of visceral adipose tissue. Our results suggest paternally expressed genes in PWS/AS locus play a significant role for the obesity and identify new potential targets for future research and treatment of obesity.

Introduction

The obesity epidemic is becoming a global phenomenon. In 2008, the World Health Organization (WHO) reported that 35% of adults over 20 years old were overweight and 11% were obese (1) and that the worldwide rate of obesity has nearly doubled since 1980. Obesity causes many health problems, such as type 2 diabetes mellitus, hypertension and cardiovascular diseases (2–4). Direct causes of obesity are thought to be a combination of excessive food intake and/or lack of physical activity, however, the underlying mechanism often includes genetic factors. It has been estimated that the genetic heritability of obesity is 40–70% from twin studies (5). Furthermore, some genetically modified (engineered) mutant mice show increased susceptibility to obesity at either normal or high-fat diet (HFD) (6). The understanding of genetic underpinning of obesity is important for the prevention and medical intervention of obesity.

Prader–Willi syndrome (PWS; OMIM #176270) is one of the most well-known obesity-related syndromes caused by genetic factors. PWS patients exhibit short stature, cognitive impairment and most prominently, morbid obesity induced by hyperphagia (7). PWS is a result from loss or inactivation of

[†]These authors have equally contributed to this work.

Received: December 10, 2014. **Revised and Accepted:** May 18, 2015

contiguous genes in paternal allele of chromosome 15q11–q13. About 70% cases of PWS have a large interstitial deletion (–6.8 Mb) in the paternal allele, 25% have maternal uniparental disomy and 3% show a mutation in the specific genomic region, called the imprinting center (IC) (8,9). Deletion of the same region on the maternal allele causes Angelman syndrome that exhibits intellectual disability and ataxia without showing obesity (10,11). To identify the obesity responsible genes in the PWS/AS locus, several studies have been conducted using human genetics or genetic-engineered mouse models (12,13). However, current 15q11–q13 deletion mouse models do not mimic the obese phenotypes in PWS well.

Duplication of the 15q11–q13 region is one of the most frequent chromosomal aberrations for autism spectrum disorders (ASD) (15q11–q13 duplication syndrome, OMIM: #608636). The majority of 15q11–q13 duplication syndrome cases result from a maternally inherited duplication (14,15). However, recent reports showed that a paternally inherited duplication can also cause several ASD features such as development/speech delay or mental retardation (16). Although the number of cases is still limited, interestingly, several patients with paternally inherited duplication or triplication of the PWS/AS locus display PWS-like features including obesity or hypotonia (17–22). These findings raise the possibility that the increased gene dosage in this region might contribute to obesity in addition to deletion of this region.

In our previous studies, using a chromosome engineering technique, we generated mice with an interstitial duplication of 6 Mb on mouse chromosome 7B-C that corresponds to human chromosome 15q11–q13 (23–25). We found that mice, inherited this duplication from their father (*patDp/+*), displayed several behavioral abnormalities resembling autism. In this study, we demonstrated that *patDp/+* (but not *matDp/+*) mice displayed late-onset obesity without affecting food intake and examined the mechanism by which *patDp/+* mice develop obesity.

Results

patDp/+ mice show late-onset obesity, increased fat mass and higher sensitivity to HFD

We previously reported that *patDp/+* mice display normal growth until adulthood and that the body weight of *patDp/+* mice is comparable to that of wild-type (WT) mice (23). However, *patDp/+* mice older than 20 weeks start to show clear obese phenotypes, even when fed regular chow (RC) (Supplementary Material, Fig. S1). In the present study, we performed detailed analyses of the obese phenotypes of *patDp/+* mice. To evaluate obese phenotypes in *patDp/+* mice, we first examined the effect of an HFD on body weight and fat mass in *patDp/+* male mice. The repeated measures of analysis of variance (ANOVA) model revealed significant difference in main effects of genotype ($P = 0.02$), food ($P < 0.01$) and time ($P < 0.01$) (Fig. 1A). HFD-treated *patDp/+* mice rapidly showed significantly increased body weight compared with HFD-treated WT control animals (Fig. 1A), already after 4–6

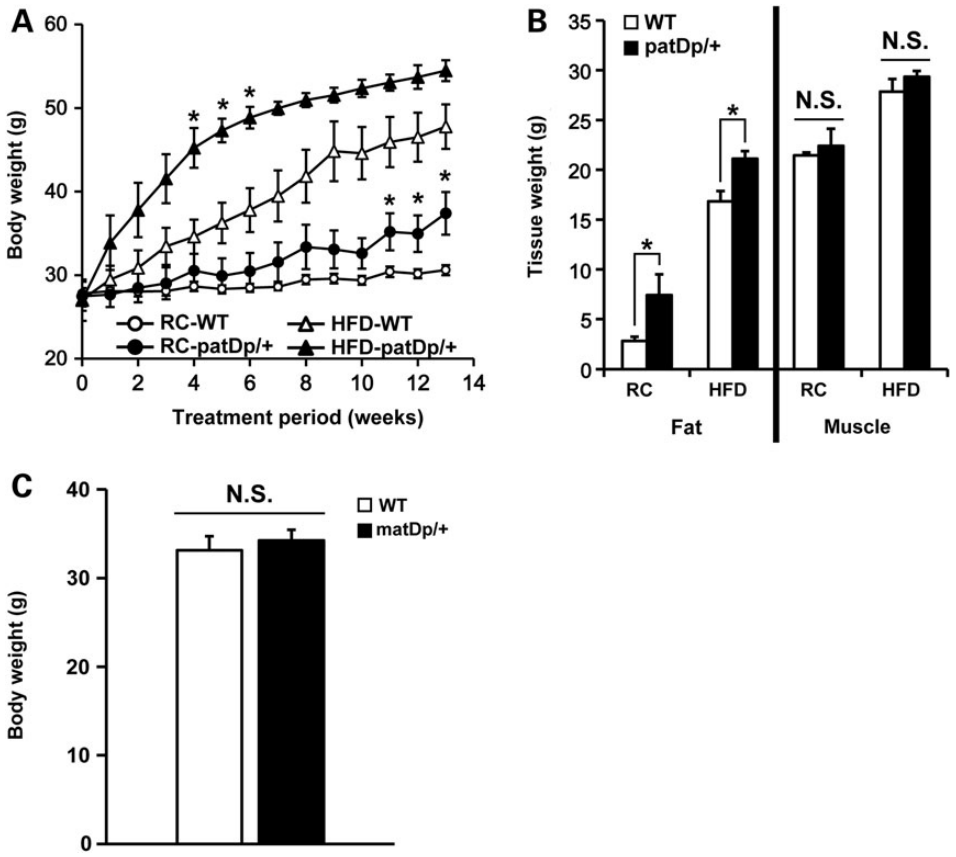

Figure 1. Body weight and composition analysis in male *patDp/+* mice. (**A**) Effect of HFD to body weight. Designated animals were fed RC or HFD for 13 weeks ($N = 3$–6 for each group). A repeated measure of the ANOVA model applied to this data (Genotype $P < 0.05$ and food $P < 0.01$). (**B**) Body composition analysis. After treatment of RC or HFD for 14 weeks, the amount of fat and muscle were measured by NMR ($N = 3$–7 for each group). (**C**) Body weight of *matDp/+* male mice. Twenty-two-week-old male mice were used for this analysis ($N = 9$ for each genotype). Values are the mean and error bars represent the standard error of the mean (SEM). *$P < 0.05$, N.S. represents not significant difference ($P > 0.05$).

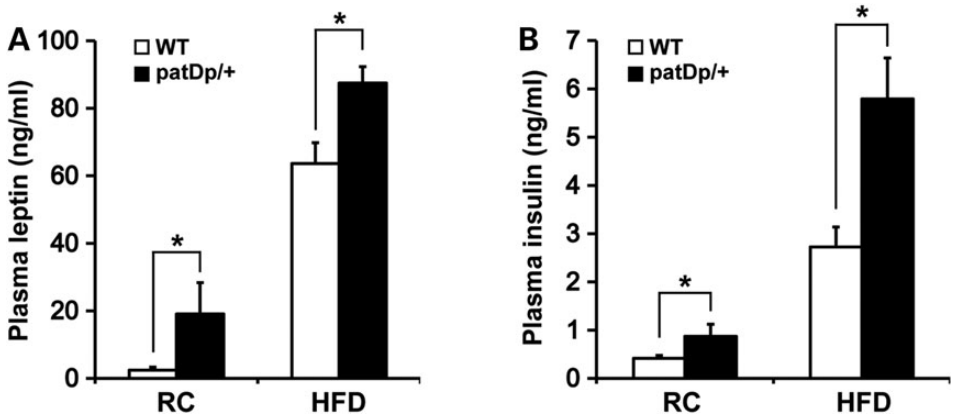

Figure 2. Plasma leptin and insulin levels in male *patDp/+* mice with RC or HFD. (**A** and **B**) Plasma leptin and insulin levels were verified by ELISA-based assay (N = 3–7 for each group). Values are the mean and error bars represent the SEM. *P < 0.05.

weeks treatment (4 weeks; HFD-WT: 34.6 ± 2.0, HFD *patDp/+*: 45.2 ± 2.4 g). Even in groups fed with RC, *patDp/+* mice showed increased body weight (Fig. 1A), although after a longer treatment period (11–13 weeks; 13 weeks; RC-WT: 30.6±0.6, RC-*patDp/+*: 37.4 ± 2.6 g). We then examined body composition analysis by using nuclear magnetic resonance (NMR) to measure fat and lean mass quantitatively. Fat mass was significantly higher in *patDp/+* mice than in WT mice under both RC and HFD conditions while there was no significant difference in body muscle content (Fig. 1B). Additionally, *matDp/+* mice in which the same chromosomal duplication is derived from maternal allele did not show late-onset obesity (Fig. 1C).

We further investigated if blood parameters in aged or HFD *patDp/+* male mice correlated with body weight or fat mass. We measured two key hormones that regulate obesity, insulin and leptin. Consistent with the increased fat mass, both plasma leptin and insulin were significantly elevated in *patDp/+* mice under both RC and HFD conditions after 13 weeks (Fig. 2). We also investigated the effect on a HFD for *patDp/+* female mice (Supplementary Material, Fig. S2). In HFD-treated female mice, *patDp/+* mice showed increased body weight, fat content, plasma leptin and insulin compared with WT while *matDp/+* mice did not show any significant difference. However, there were no significant differences in any parameters including body weight, fat content and plasma hormones in the case of RC. Taken together, these results indicate that the increased body weight in *patDp/+* mice found at the aged stage is due to expansion of adipose tissue and that *patDp/+* (but not *matDp/+*) mice have a genetic susceptibility to HFD-induced obesity. To find the primary effects of the underlying genetic factors and exclude secondary effects resulting from obesity, we used young adult (8–10 weeks old) mice for further study. At this stage, we found no significant difference in body weight between *patDp/+* and WT mice (see Fig. 3B, feed time = 0).

patDp/+ mice have normal levels of energy balance

Genetically modified mice to model obesity or resistance to obesity often have altered energy expenditure (26–28). Therefore, we measured locomotor activity and respiratory quotient (RQ) of *patDp/+* mice. A slight reduction of locomotor activity in *patDp/+* mice during the light phase was observed, but it was not statistically significantly different compared with WT mice (Supplementary Material, Fig. S3A). Furthermore, oxygen consumption, carbon dioxide production and RQ were not significantly different between *patDp/+* and WT mice (Supplementary Material, Fig. S3B–D). These results suggest that the energy expenditure is unlikely to be a major factor in the late-onset obesity found in *patDp/+* mice.

Food intake is not a major reason for obesity found in *patDp/+* mice

To further investigate the causes of obesity in *patDp/+* mice, we next measured food intake and body weight under *ad libitum* feeding conditions. Increased food intake, hyperphagia, is one of the most frequent causes for general obesity and leads to obesity in the later childhood of PWS (29). WT and *patDp/+* mice used in this analysis were of the same age (8 weeks old), sex (male) and environment (littermate). At the initial stage of the analysis, they showed similar body weight (WT: 20.9 ± 0.3, *patDp/+*: 20.7 ± 0.4 g; difference not significant $P > 0.05$). During the test time (16 weeks) in *ad libitum*-fed conditions, there was no significant difference in food intake between WT and *patDp/+* mice (Fig. 3A, genotype effect, $P > 0.05$). The body weight of both genotypes was similar until 5 weeks from start (Fig. 3B), however, *patDp/+* mice started to increase body weight from 6 weeks (14 weeks old) compared with WT and the difference became larger over time (Fig. 3B). After 16 weeks (24 weeks old), the difference in body weight became significant (WT: 29.6 ± 0.5, *patDp/+*: 34.5 ± 1.4 g) while food intake remained comparable.

Additionally, we performed pair-fed analysis. In this analysis, we set the amount of food for all mice to the same one (Fig. 3C). In this experimental condition, mice received slight restriction of food during the test time as a whole. As a result, WT mice started to lose their body weight from 2 weeks (Fig. 3D). On the contrary, *patDp/+* mice kept on their body weight during the test period (Fig. 3D). These results indicate that the late-onset obesity seen in *patDp/+* mice is unlikely to be due to the increased food intake and that *patDp/+* mice are resistant to food restriction.

Young adult *patDp/+* mice have enlarged white adipocytes

We next performed histological analysis of white adipose tissue (WAT) in *patDp/+* mice because aged *patDp/+* mice contained prominent abdominal visceral fat (Fig. 1B, RC). First, we observed white adipocytes in aged mice with age of over 20 weeks and larger body weight than WT mice. As we expected, aged *patDp/+* contained a greater number of enlarged adipocytes, compared

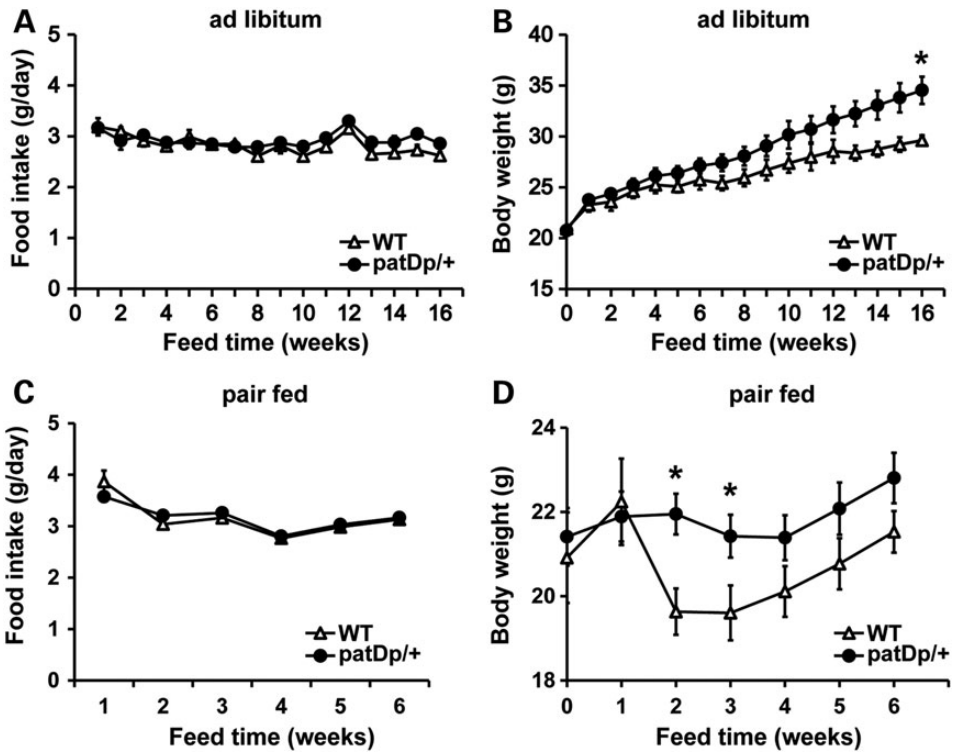

Figure 3. Food intake in *ad libitum* condition and pair-fed examination. (**A** and **B**) Food intake and body weight under *ad libitum* condition ($N = 3$–4 mice for each genotype). 'Feed time 0' means 8 weeks old. (**C** and **D**) Under pair-fed condition, food intake and body weight were measured in male WT or *patDp*/+ mice fed RC ($N = 3$–4 for each genotype). Values are the mean and error bars represent the SEM. *$P < 0.05$.

with WT mice (Supplementary Material, Fig. S4). We also performed the same analysis at the young adult stage between 9 and 11 weeks. Surprisingly, even before exhibiting obesity, *patDp*/+ mice had larger adipocytes compared with WT mice (Fig. 4A). We further used Adiposoft to determine the size of adipocytes automatically and objectively (30). The animals used in this analysis had equivalent body weights (WT: 26.1 ± 1.1, *patDp*/+: 26.7 ± 0.6 g). The peak of adipocyte area was about 900–1200 μm^2 in both genotypes. But larger adipocytes were dominant in *patDp*/+ mice in the distribution analysis (Fig. 4B). In fact, the median of adipocyte size was significantly larger in *patDp*/+ mice (Fig. 4C). These data indicate that hypertrophy of white adipocytes in *patDp*/+ mice precedes the gain of body weight.

Sfrp5 is up-regulated prior to the onset of obesity

To identify abnormal molecular signaling in *patDp*/+ mice with an unbiased approach, we performed gene expression profiling in WAT. To exclude the after effect of obesity again, we chose the young adult stage when body weight was not different between genotypes. After processing the raw data obtained by Agilent microarray, expression difference between WT and *patDp*/+ mice was analyzed by Volcano plot analysis (Fig. 5A). We first set relatively mild criteria to extract differentially expressed genes (DEGs) for pathway analysis ($P < 0.05$ by moderated *t*-test, fold change >1.3) and top 20 DEGs were listed (Tables 1 and 2). Extracted DEGs were used for network analysis by Ingenuity Pathway Analysis (IPA) software to identify relevant biological networks or pathways in *patDp*/+ mice (Fig. 6 and Table 3). The top score network was 'Energy Production, Lipid Metabolism, Small Molecule Biochemistry'. This result suggests metabolic pathways of white adipocytes in *patDp*/+ are altered compared with WT mice. Thus, we postulated that abnormal signaling in WAT may contribute to induce obesity in *patDp*/+ mice. To investigate this hypothesis and to identify the *bona fide* causative gene, we used more stringent criteria for extracting DEGs ($P < 0.01$ by moderated *t*-test, fold change >1.5, depicted in Fig. 5A, Tables 1 and 2). DEGs included paternally expressed genes (PEGs) *Ndn*, *Snurf* and *Snrpn* that were located within the duplicated region (mouse chromosome 7B-C region), indicating the DEGs list was reliable (Fig. 5A). Among identified DEGs, Secreted frizzled-related protein (*Sfrp*) family members, especially *Sfrp5*, were particularly relevant. First, *Sfrp5* is expressed in adipocytes and is strongly induced during adipocyte differentiation (31). Secondly, up-regulation of *Sfrp5* is correlated with weight gain (32). Finally, SFRP5-deficient mice show opposite phenotypes to *patDp*/+ mice such as resistance to HFD-induced obesity, lower amount of fat, reduced adipocyte size without affecting food intake, locomotor activity and RQ (33). To confirm the up-regulations of *Sfrp5* and the genes located in duplication region in *patDp*/+ WAT, we performed the quantification of RNA expressions in *patDp*/+ and *matDp*/+ mice by quantitative polymerase chain reaction (qPCR) analysis. *Sfrp5* expression was increased only in *patDp*/+ mice but not in *matDp*/+ mice (Fig. 5B). PEGs including *Ndn* and *Snrpn* were increased in *patDp*/+ WAT in the same way as in brain (Supplementary Material, Fig. S5). This result suggests that increased *Sfrp5* gene may have a substantial role in the obese phenotypes observed in *patDp*/+ mice and PEGs are implicated in these phenotypes.

Generation and validation of 3 Mb duplication mice

The late-onset obesity found in *patDp*/+ mice was not observed in *matDp*/+ mice (Fig. 1B and C), suggesting that genomic imprinting

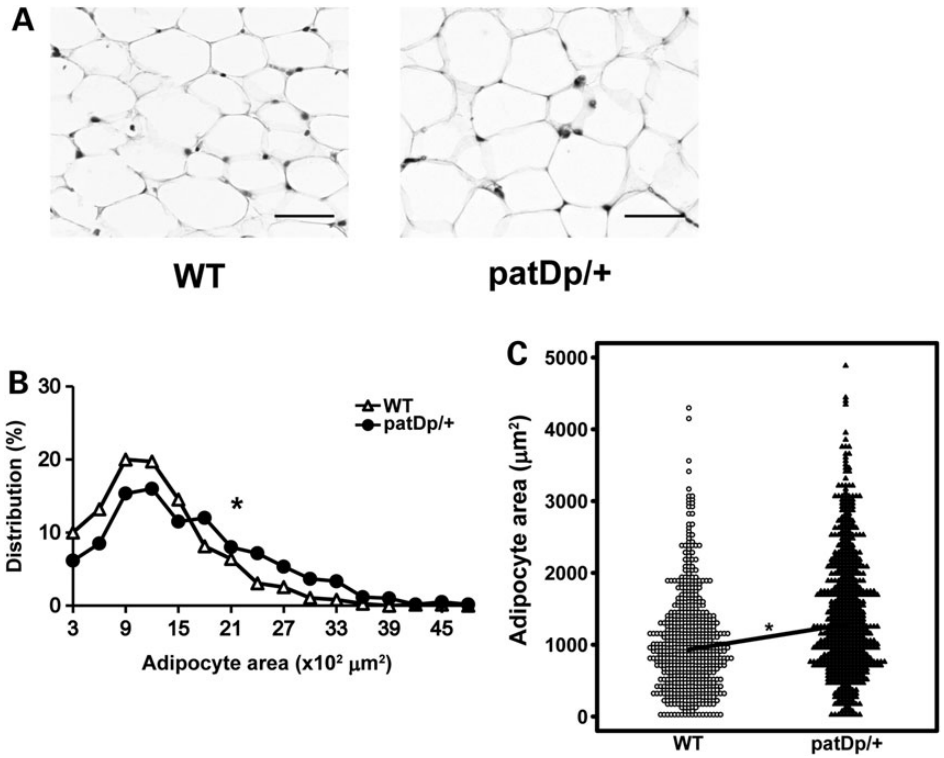

Figure 4. Histological investigation of WAT before manifesting obesity in male *patDp/+* mice. (**A**) Representative white adipocytes stained with hematoxylin–eosin (HE). The mice used for this analysis had almost the same body weight before manifesting obesity. Scale bars represent 50 μm. (**B**) Distribution of the size of white adipocytes. Distribution difference between two genotypes was evaluated by Kolmogorov–Smirnov test. *$P < 0.01$. (**C**) Measured size of adipocytes was compared with WT mice. White circle and black triangle indicate each adipocyte from WT and *patDp/+* mice, respectively. A line means median for each genotype. The number of mice used in this analysis was four for each genotype and 150 adipocytes were used for each mouse. *$P < 0.01$ (Mann–Whitney *U* test).

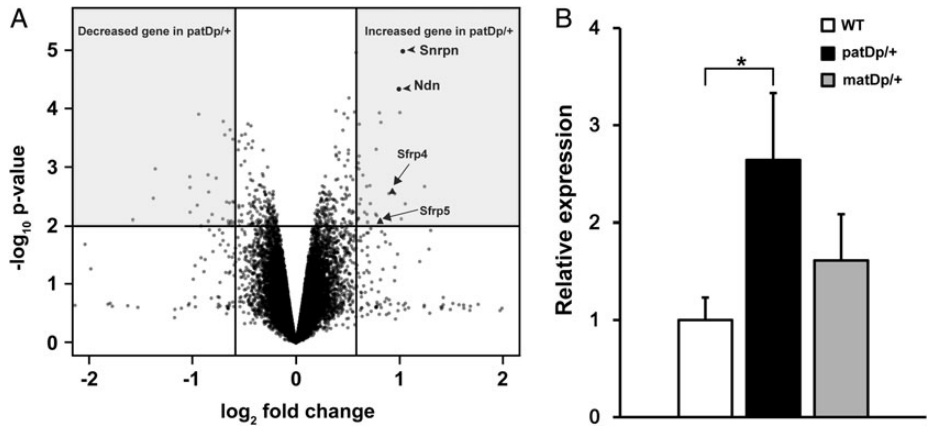

Figure 5. Gene expression profiling of WAT before manifesting obesity in male *patDp/+* mice. (**A**) A volcano plot from the result of gene expression profiling of WAT ($N = 3$ for each genotype). Vertical lines represent 1.5-fold change and a horizontal line means $P < 0.01$ (moderated t-test). Arrowheads indicate *Snrpn* and *Ndn* genes located inside of duplicated chromosomal region. Arrows mean the *Sfrp* family as a candidate for obesity in *patDp/+* mice. (**B**) Expression of *Sfrp5* mRNA in WAT before manifesting obesity in *patDp/+* mice ($N = 9$ for WT, 5 for *patDp/+* and *matDp/+* mice, respectively). Averaged WT expression level set to 1 and *Actb* gene was used as an internal control. Male mice were used for this analysis (10–13 weeks old). Values are the mean and error bars represent SEM. *$P < 0.05$ significantly different from WT mice by Tukey–Kramer test.

might be involved in the development of the obese phenotypes. It is likely that PEGs present in the duplicated locus play an initiating role in this obesity. To test this hypothesis, we generated mice carrying a partial duplication of the PWS/AS locus with an *in vivo* chromosomal engineering technique (Fig. 7A) (34). The newly generated mice contained an interstitial duplication of about 3 Mb genome from *Ube3a* to the upstream region of *Ndn* (mm9: chr7 66,254,803–69,306,344), while original duplication mice (*patDp/+*) had about 6 Mb genome including from *Herc2* to *Mkrn3* (mm9:chr7 63,251,692–69,599,917). *patDp/+* mice with

Table 1. Top 20 genes up-regulated in WAT of *patDp/+* mice

Gene symbol	Gene name	Accession number	Fold change	P-value
Acta1	Actin alpha 1	NM_009606	2.367	0.002
Ccl7	Chemokine (C-C motif) ligand 7	NM_013654	2.080	0.004
Snrpn	Small nuclear ribonucleoprotein	NM_013670	2.046	<0.001
Ndn	Necdin (Ndn)	NM_010882	1.991	<0.001
Tmem45b	Transmembrane protein 45b	NM_144936	1.940	0.003
Sfrp4	Secreted frizzled-related protein 4	NM_016687	1.904	0.003
Sfrp5	Secreted frizzled-related sequence protein 5	NM_018780	1.758	0.009
Snurf	SNRPN upstream reading frame (Snurf)	NM_033174	1.750	<0.001
Thbs1	Thrombospondin 1	NM_011580	1.717	0.007
Ctgf	Connective tissue growth factor	NM_010217	1.707	0.006
Pamr1	Peptidase domain containing associated with muscle regeneration 1	NM_173749	1.642	0.002
Egr2	Early growth response 2	NM_010118	1.616	0.009
Timp1	Tissue inhibitor of metalloproteinase 1	NM_001044384	1.609	0.006
Dact2	Dapper homolog 2, antagonist of beta-catenin	NM_172826	1.584	0.006
Cryab	Crystallin, alpha B	NM_009964	1.566	0.001
Sirpb1b	Signal-regulatory protein beta 1B	NM_001173460	1.531	0.004
Slc1a1	Solute carrier family 1 member 1	NM_009199	1.529	<0.001
Atp10a	ATPase, class V, type 10A	NM_009728	1.529	0.001
Pdlim7	PDZ and LIM domain 7	NM_026131	1.526	0.001
Npr3	Natriuretic peptide receptor 3	NM_008728	1.521	0.008

Table 2. Top 20 genes down-regulated in WAT of *patDp/+* mice

Gene symbol	Gene name	Accession number	Fold change	P-value
Fndc5	Fibronectin type III domain containing 5	NM_027402	0.336	0.0080
Mmd2	Monocyte to macrophage differentiation-associated 2	NM_175217	0.492	0.0023
Rgs2	Regulator of G-protein signaling 2	NM_009061	0.522	<0.001
H2-Q10	Histocompatibility 2	NM_010391	0.556	0.0084
Tst	Thiosulfate sulfurtransferase	NM_009437	0.571	0.0065
Ptgds	Prostaglandin D2 synthase	NM_008963	0.587	0.0016
Hpca	Hippocalcin	NM_010471	0.613	0.0078
Sfrp1	Secreted frizzled-related protein 1	NM_013834	0.621	<0.001
Apod	Apolipoprotein D	NM_007470	0.629	0.0040
Pappa	Pregnancy-associated plasma protein A	NM_021362	0.638	0.0093
Prnd	Prion protein dublet	NM_023043	0.641	0.0041
1500015O10Rik	RIKEN cDNA 1500015O10 gene	NM_024283	0.644	<0.001
Cpxm2	Carboxypeptidase X 2	NM_018867	0.645	0.0090
Nmb	Neuromedin B	NM_026523	0.648	0.0084
Agpat9	1-acylglycerol-3-phosphate O-acyltransferase 9	NM_172715	0.656	0.0039
Dennd2d	DENN/MADD domain containing 2D	NM_028110	0.662	0.0040
Sox9	SRY-box containing gene 9	NM_011448	0.680	<0.001
Igfbp2	Insulin-like growth factor binding protein 2	NM_008342	0.683	0.0046
Ppargc1a	Peroxisome proliferative activated receptor	NM_008904	0.683	0.0050
Avpr1a	Arginine vasopressin receptor 1A	NM_016847	0.683	0.0084

3 Mb duplication (3 Mb *patDp/+*) showed normal viability and fertility, like *patDp/+ mice* with 6 Mb duplication (6 Mb *patDp/+*) (23). First, we checked if unexpected deletions or duplications occurred during chromosome engineering by using high-resolution array comparative genomic hybridization (aCGH) (Fig. 7B). We only detected increased copy number in the expected genomic region (upstream of *Snrpn* to intergenic between *Ube3a* and *Atp10a*) in 3 Mb *patDp/+* mice. These results indicate there are no unexpected chromosomal aberrations. Next, we tested with qPCR how RNA expression levels in the brain, where the imprinted expression is well known, were impacted by changes in the gene copy number in detail. As expected, in 3 Mb *patDp/+* mice, the expression levels of PEGs located within the duplicated region, such as *Snrpn*, *Snord116* and *Snord115* were 1.5–2-fold increased (expressed from two copies) as much as WT (expressed from one copy) and the genes located outside the duplicated region, like *Mkrn3* and *Gabrb3* were comparable levels to WT mice (Fig. 7C). However, unexpectedly, the expression of *Ndn* was decreased compared with WT mice although *Ndn* is located outside the duplicated region. The expression of *Ube3a* was slightly elevated in 3 Mb *patDp/+* mice. Furthermore, we performed the same analysis on 3 Mb *matDp/+* mice (Fig. 7D). In 3 Mb *matDp/+* mice, only *Ube3a* expression was increased as expected. These results suggest the gene expressions within the duplicated region were increased depending on the copy number and imprinting manner. These data are consistent with other reports that *Ube3a* mRNA in the brain is expressed only from maternal chromosome (35–38).

Three Mb *patDp/+* mice recapitulate the late-onset obesity found in 6 Mb *patDp/+* mice

We measured body weight of 3 Mb *patDp/+* and *matDp/+* mice. The abdominal visceral fat clearly increased in 3 Mb *patDp/+* mice (data not shown). Similar to 6 Mb *patDp/+* mice, 3 Mb *patDp/+* mice also showed late-onset obesity (Fig. 8) while 3 Mb *matDp/+* mice did not show obesity and have similar body weight compared with WT mice (Fig. 8). We also checked the gene expression levels in 3 Mb *patDp/+* and *matDp/+* WAT and found only *Snrpn* was up-regulated in 3 Mb *patDp/+* while *Ube3a* was up-regulated only in 3 Mb *matDp/+* mice (Supplementary Material, Fig. S6). These results showed that 3 Mb *patDp/+* mice recapitulated the obese phenotype found in 6 Mb *patDp/+* mice. It strongly suggests that increased expression of the PEGs present within the region of 3 Mb is responsible for the resulting obesity.

Discussion

Difference in locomotor activity does not explain obesity in *patDp/+* mice

The present study demonstrated that *patDp/+* mice with paternally inherited duplication in PWS/AS locus showed late-onset obesity caused by adipocyte hypertrophy, hyperleptinemia and hyperinsulinemia in RC condition. Importantly, there was no change in food intake or RQ in *patDp/+* mice. Our previous study suggested that *patDp/+* mice might have decreased locomotor activity (24) and in this study we also observed a slight—but not statistically significant—tendency to decreased locomotor activity in *patDp/+* (Supplementary Material, Fig. S3A). Hence, we cannot completely exclude the possibility that reduced locomotor activity may contribute to the obesity found in *patDp/+* mice. However, late-onset obesity was found in almost all *patDp/+* mice while their reduced locomotor activity was relatively weak and less frequent than obesity seen in *patDp/+* mice. Furthermore, although 3 Mb *patDp/+* mice showed clear obesity, they displayed normal locomotor activity at least in a novel environment (Supplementary Material, Fig. S7). Taken together, our observation argues that reduction of locomotor activity in *patDp/+* mice is unlikely to be the major cause of obesity.

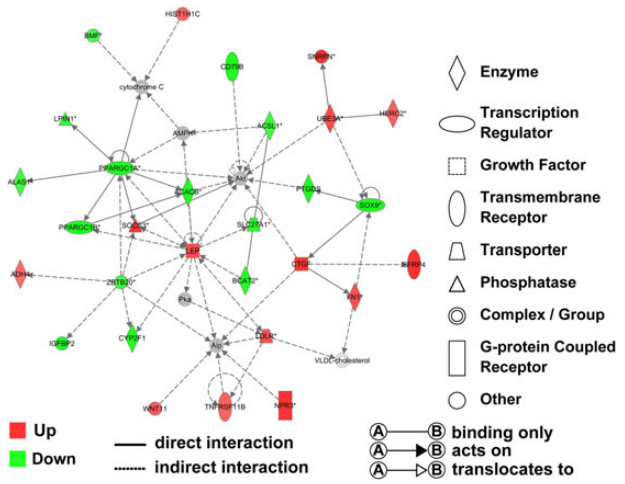

Figure 6. Network analysis of WAT in male *patDp/+* mice. Network analysis of the DEGs ($P < 0.05$, fold change >1.3) between *patDp/+* and WT mice. Top ranked, Network 1 analyzed by IPA was presented. Each network shows genes and its products as nodes. The shapes of node are defined according to its function or localization. Lines between each node mean biological relationships, such as protein–protein interaction or transcriptional regulation. The color intensity of each node indicates the degree of up-regulation (red) and down-regulation (green) in *patDp/+* mice compared with WT mice. Gray color means no change. Asterisks indicate redundant probes converged.

Relationships between PWS–autism and deletion–duplication from the aspect of obesity

Several recent studies implicated that ASD was more prevalent in PWS than previously recognized (39–41), though maternal duplication of this region has been thought to have a primary role in ASD. Actually, it was reported that truncating mutations of the PWS-responsible gene, *MAGEL2*, were found in PWS with ASD (42). Our data together with these reports suggest that deletion and duplication of PWS/AS locus, especially PEGs, share the molecular pathways of pathophysiology of obesity. Understanding of the pathways will reveal the discrepancy of obese phenotypes between model mice of deletion and duplication.

PEGs in 3 Mb region as a possible role in obesity

Until now, over 30 lines of model mice for PWS have been generated to identify the responsible genes (12,13). Each mutant mouse model partly showed features seen in PWS patients. Recent human genetic studies identified in PWS patients the translocation (43,44) and microdeletion (45–47) of *SNORD116*, a small nucleolar RNA (snoRNA) located on PWS/AS locus. To assess the role of this gene for PWS, *Snord116* deletion mice were generated and analyzed (48–51). These studies showed that *Snord116* deletion mice displayed failure to thrive with poor sucking of milk, late-onset hyperphagia and hyperghrelinemia, which are common symptoms in PWS patients (48,49,52). However, all of the model mice for PWS, including *Snord116* deletion mice, did not show obesity. From these aspects, the clear obesity phenotype shown by 6 and 3 Mb *patDp/+* mice is intriguing and these mice will be invaluable models of obesity in the PWS/AS locus. Several individuals with paternally inherited duplication or triplication in PWS/AS locus exhibited PWS-like features including obesity (17–19,21,22,39). On the other hand, there are some distinct features between PWS and our duplication models. PWS individuals showed the amount of visceral fat and fasting insulin level were decreased when it was compared with 'obese controls' (53) while

Table 3. Result of network analysis with IPA

ID	Associated network functions	Score
1	Energy production, lipid metabolism, small molecule biochemistry	44
2	Cell-to-cell signaling and interaction, cellular movement, hematological system development and function	33
3	Connective tissue disorders, metabolic disease, cell morphology	20
4	Reproductive system development and function, cellular growth and proliferation, endocrine system development and function	18
5	Cell-to-cell signaling and interaction, tissue development, hematological system development and function	17

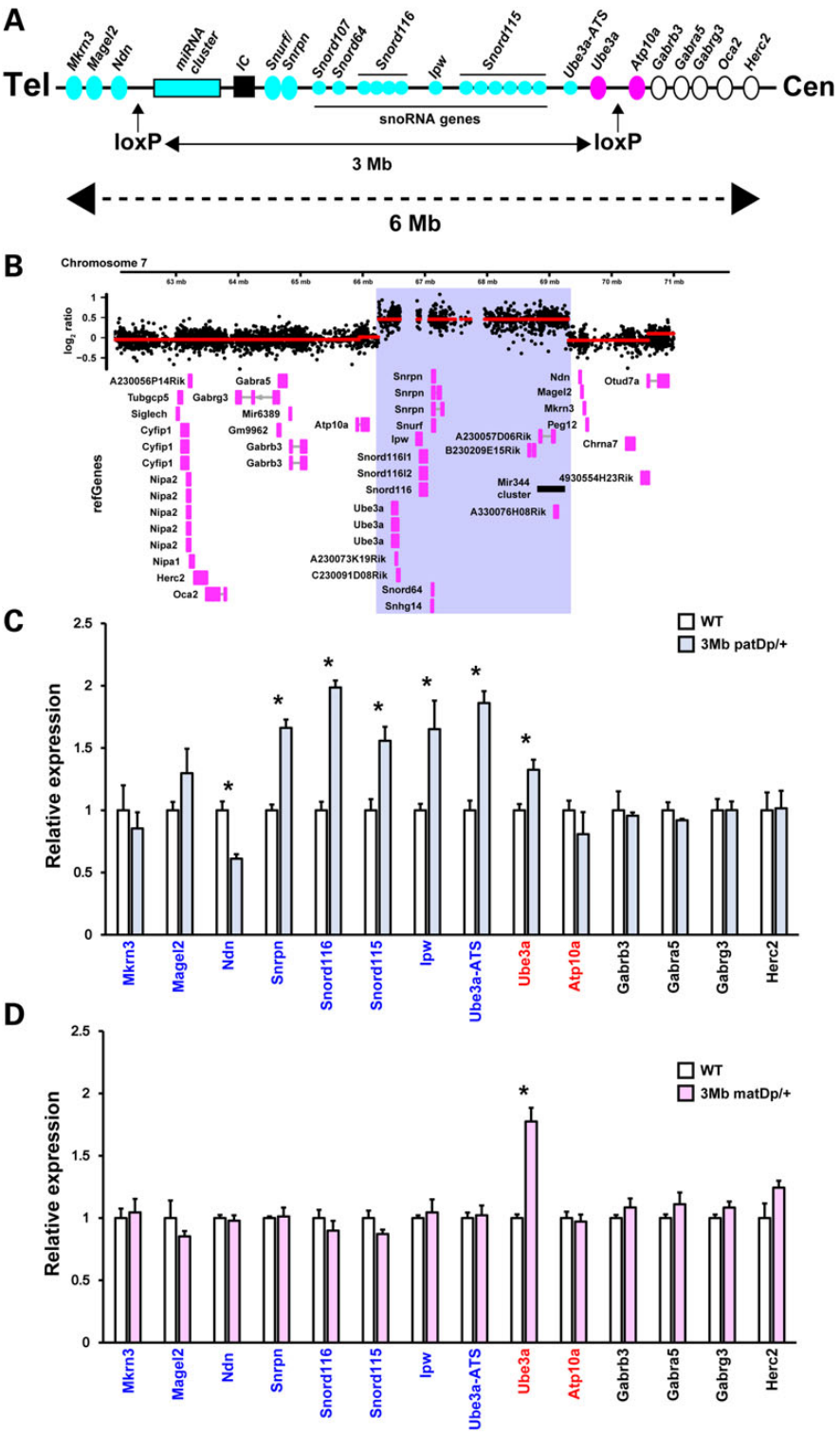

Figure 7. Generation of mice with 3 Mb duplication within PWS/AS chromosomal region. (**A**) A schematic view of PWS/AS region and target region for duplication. The original 6 Mb duplication mice contain duplicated chromosome from *Herc2* to *Mkrn3* (proximal to distal) while new 3 Mb duplication mice contain that from *Ube3a* to miRNA cluster region. Blue, pink and white circles indicate paternally, maternally and biallelically expressed genes, respectively. A blue box indicates an miRNA cluster. A black box, labeled 'IC' means imprinting center. Tel and Cen indicate telomere and centromere. (**B**) Copy number analysis of DNA isolated form 3 Mb *patDp/+* mice by high-resolution array comparative genomic hybridization (aCGH). Pink box indicates each exon of the genes obtained from UCSC genome browser. Blue shaded region represents the duplicated chromosome. The genome DNA from WT mouse was used as reference DNA and plotted are $\log_2$-transformed signal ratio of 3 Mb *patDp/+* to WT mouse. Base-pair position along mouse chromosome 7 was described horizontally (mm9). Red lines represent the estimated mean of each segment. (**C** and **D**) The mRNA expressions in 3 Mb *patDp/+* (C) and *matDp/+* (D) mice were measured by RT–qPCR. Each value was normalized by *Gapdh* as an internal control and described as a relative value to WT expression ($N = 4$–5 for each genotype). Adult hippocampi were used for comparison with WT mice for each gene, except for *Magel2* because of its undetectable expression. For *Magel2*, hypothalamus was used for quantification. Blue, red and black genes indicate paternally, maternally and biallelically expressed genes, respectively. Values are the mean and error bars represent the SEM. $^*P < 0.05$.

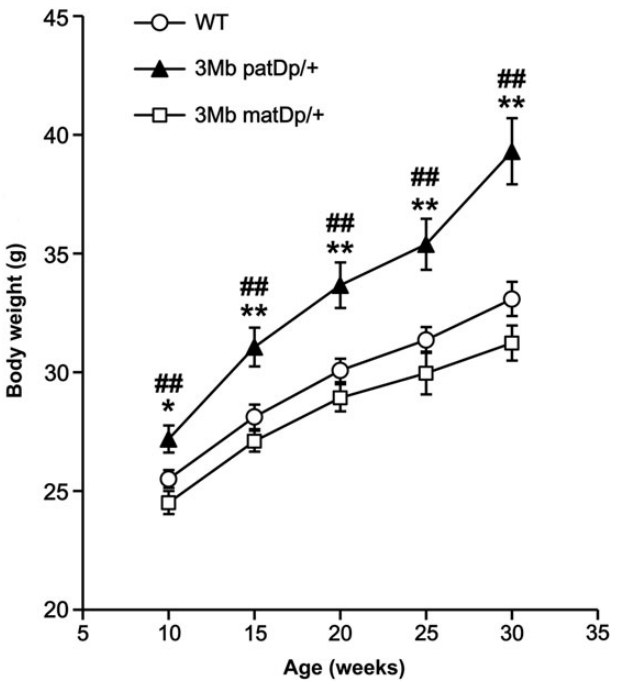

Figure 8. Body weight of 3 Mb *patDp/+* and *matDp/+* male mice. Measurement of body weight in 3 Mb *patDp/+* and *matDp/+* male mice (N = 13 for WT, 7 for 3 Mb *patDp/+* and 8 for *matDp/+* mice, respectively). Values are the mean and error bars represent SEM. $^{*}P < 0.05$, $^{**}P < 0.01$ significantly different from WT mice and $^{\#}P < 0.05$, $^{\#\#}P < 0.01$ significantly different from 3 Mb *matDp/+* mice by Tukey–Kramer test.

both 6 and 3 Mb *patDp/+* mice showed clear increased adiposity (Fig. 1B and data not shown). Thus, there might be different mechanisms of obesity between deletion and duplication.

The 3 Mb duplication mice we generated in this study have an additional copy number of several genes, including snoRNAs, *Snurf-Snrpn* and *Ube3a*. Since 6 and 3 Mb *matDp/+* mice did not show obesity (Figs 1C and 8), the involvement of the maternally expressed *Ube3a* gene can be excluded. Among the remaining genes, *Snord116* is the most plausible gene related to the obesity as discussed earlier. Nonetheless, we still cannot exclude *SNORD115/Snord115* as another candidate gene for obesity. *Snord115* gene was also diminished both in PWS patients and model mice for PWS including large deletion models (54,55). Although deletion of this gene did not show obesity or other PWS features in the previous study (56), this gene has been reported to play a role in RNA editing and alternative splicing of serotonin 2C receptor (*Htr2c*) (23,54,57–59). Loss of function for *Htr2c* in mice was reported to exhibit hyperphagia and late-onset obesity (60). More importantly, Kawahara *et al.* (61) generated two independent *Htr2c*-related mutant mice with 5-HT_{2C}R-INI (editing blocked) and VGV (fully edited) forms in *Htr2c*. The mice with VGV form of 5-HT_{2C}R showed severely reduced fat mass and increased energy expenditure as well as hyperphagia while the mice with INI form grew normally. Indeed, both 6 and 3 Mb *patDp/+* mice showed increased *Snord115* expression and 6 Mb *patDp/+* mice exhibited increased RNA editing ratio in *Htr2c* (23).

Johnstone *et al.* (62) produced PWS-IC^{Hs} mice that have a targeted replacement of the mouse PWS-IC with human PWS-IC. Maternal inheritance of this allele (PWS-$IC^{Hs/+}$) caused unsilencing of *Snrpn* and *Snord* family expression in this locus without affecting *Ndn*, *Magel2* and *Mkrn3* expressions. Supporting our results, PWS-$IC^{Hs/+}$ mice showed overgrowth. However, the overgrowth in PWS-$IC^{Hs/+}$ is thought to be caused by two possibilities. They have repressed expression of *Ube3a* by 2-fold increased expression of *Ube3a-ATS* and 2-fold increased expression of *Snrpn* and *Snord* family. Because maternal *Ube3a* depleted mice also have been reported to show overgrowth (63,64) and Angelman syndrome individuals caused by uniparental disomy or imprinting defect show increased body mass index (65), the reduction of *Ube3a* expression could be a candidate for the obesity. On the other hand, in the present study, 6 and 3 Mb *patDp/+* mice showed obesity without reducing *Ube3a* expression both in the brain and WAT (Fig. 7C and Supplementary Material, Figs S5 and S6), suggesting that PEGs in 3 Mb region including *Snrpn* or *Snord* family are reliable candidates for obese phenotypes. Further evaluation will be required to determine how these imprinting regions contribute to obesity and which snoRNA plays a critical role in the obesity found in duplication mice.

Altered signaling of lipid metabolism and Sfrp dysregulation in WAT as a possible cause for obesity in *patDp/+* mice

The identification of the cause of obesity in forward genetic manner is still challenging because it is hard to distinguish if the phenotypes found in experiments are effects or causes of obesity. To avoid the secondary effect of obesity, we chose young adult stage for gene-expression profiling. This result revealed altered lipid metabolism and energy production pathway in *patDp/+* mice. The DEGs in this analysis included several *Sfrp* gene family; *Sfrp1* mRNA was decreased and *Sfrp4* and *Sfrp5* were increased in *patDp/+* mice. A well-known function of the *Sfrp* family is a negative regulator for WNT while its functions are now expanding. WNT in adipocytes can regulate several biological signaling pathways including inhibition of pre-adipocyte differentiation and suppression of adipogenesis (66,67), so altered signaling via SFRP to WNT might contribute to the obese phenotypes in *patDp/+* mice. Among the *Sfrp* family, *Sfrp5* is especially intriguing. Mori *et al.* (33) generated *Sfrp5*-deficient ($Sfrp5^{Q27stop}$) mice and revealed that they were resistant to HFD-induced weight gain, decreased fat mass, increased the number of small adipocytes, hypoleptinemia and hypoinsulinemia. These phenotypes were totally opposite to those of *patDp/+* mice with increased expression of *Sfrp5*. Importantly, these abnormal phenotypes in $Sfrp5^{Q27stop}$ mice were not due to altered food intake and respiratory exchange ratio, which is consistent with the results of *patDp/+* mice. Thus, *Sfrp5* gene might play a role as a candidate for the obesity in *patDp/+* mice.

Most of PEGs in PWS/AS region including *Snord* family are expressed in a brain-specific manner (68,69). In the present study, the expression of *Snrpn* in WAT was increased both in 6 and 3 Mb *patDp/+* mice, while no change of *Snrpn* expression in 6 and 3 Mb *matDp/+* mice was observed (Supplementary Material, Figs S5 and S6). These results implicate the involvement of *Snrpn* in WAT to obesity found in *patDp/+* mice. On the other hand, *Snrpn* knockout mice did not show obesity (70). Although the function of *Snrpn* in WAT is still not understood, the increased *Sfrp5* expression in WAT of *patDp/+* mice may be a secondary effect. Further investigation of the link between snoRNAs and SFRP would help to reveal a novel pathway to obesity.

Materials and Methods

Animals

We generated *patDp/+* mice as previously described (23). This mouse has an interstitial 6.3 Mb duplication in PWS/AS

responsible locus which is derived from the paternal allele. They were backcrossed to C57BL/6J more than 10 generations. Mice were housed in a room with a 12 h light/dark cycle (light on 8:00 a.m. and off 8:00 p.m.). Mice used in all experiments were *patDp/+* and age-matched wild-type (WT) littermates, as control (2–5 mice/cage). The experimental procedures and housing conditions for animals were approved by the Committee of Animal Experimentation, Hiroshima University (A10-74) and the RIKEN Brain Science Institute's Animal Experiments Committee. All efforts were made to minimize suffering during and after all surgeries.

HFD treatment and body composition

The mice were provided with *ad libitum* access to water and a RC (CE-2: 11.5% kcal from fat, 3.42 kcal/g, CLEA) until 9 weeks of age. At that time, half of the mice were switched to a HFD (D12492 60% kcal from fat, 5.24 kcal/g, LSG) and continued for 13 weeks. Body weight was measured weekly. After 14 weeks, body composition was analyzed by using an NMR analysis (the minispec, BRUKER).

Metabolic parameters

Plasma levels of leptin and insulin were measured by ELISA kits (Morinaga). After 18–20 h fasting, blood was collected by cardiac puncture. Then plasma was prepared by centrifugation 20 000 *g*, 15 min, 4°C.

Energy expenditure

Locomotor activity was estimated by the number of infrared beams broken in both X and Y direction (ABsystems3.02, Neuroscience Co. Ltd). The activity of individual mouse was measured in a cage (225 × 338 × 140 mm) for 10 days. Oxygen and carbon dioxide contents in 5 min were measured every 30 min for 2 days with indirect calorimetric system (Oxymax, Neuroscience Co. Ltd). During the test, mice were individually housed and had *ad libitum* access to food and water. RQ was calculated to the value V_{CO_2} divided by V_{O_2} amount.

Food intake measurement and pair-fed examination

Mice were housed individually from 8 weeks old in both paradigms. In *ad libitum* paradigm, they were provided water and RC freely. In pair-fed paradigm, all animals were controlled to feed the same amount of RC but they had access to water *ad libitum*. In both paradigms, food intake and body weight were measured every day and week, respectively.

Measurement of white adipocyte size

Mice were provided with *ad libitum* access to water and RC and were sacrificed at young adult stage between 9 and 11 weeks old because *patDp/+* mice showed almost same body weight with WT mice at this stage. WAT was dissected and transferred to 10% formaldehyde immediately. After embedding to paraffin, 4 μm sections were prepared and stained with hematoxylin–eosin. The size of adipocyte was measured by Adiposoft (30) and determined on a histological preparation by measuring the area of 150 adipocytes per each mouse. The number of mice used in this analysis was four for each genotype. Distribution difference between two genotypes was evaluated by Kolmogorov–Smirnov test.

Gene-expression profiling in WAT

Total RNA from epididymal WAT of young adult (9–10 weeks old) was extracted using TRIzol (Life Technologies), followed by column purification with DNaseI treatment (Promega). The concentration of RNA was estimated by using the NanoDrop spectrometer (Thermo) and the quality of total RNA was evaluated with Agilent 2100 Bioanalyzer (Agilent). For microarray analysis, 200 ng of total RNA was used for further procedure including Cy3 labeling with T7 RNA polymerase amplification method according to the manufacturer's instruction. Amplified and Cy3 labeled RNA was hybridized onto mouse GE 4 × 44K microarrays (G4122F) followed by washing and scanning. The raw expression data were acquired by Feature Extraction Software 9.5 (Agilent) and analyzed by Limma package (3.18.2) under the R environment (71). The signal intensities were corrected by backgroundCorrect function of the Limma package and the between arrays normalization was performed by using the quantile method. DEGs were ranked using a moderated *t*-statistic (72). Gene-expression profiling data are available from GEO (http://www.ncbi.nlm.nih.gov/geo) under accession no. GSE58191.

Network identification

Significantly DEGs (analyzed by moderated *t*-test, *P*-value <0.05 and fold change >1.3) were analyzed by Ingenuity Pathways Analysis (IPA) to identify relevant biological networks or pathways. Briefly, all DEGs along with their *P*-values and fold changes were uploaded to the IPA server (Ingenuity Systems) and were mapped as focus genes, using the Ingenuity Pathway Knowledge Base. The focus genes with highest connectivity with other focus genes were used as seed to construct core networks, and new focus genes or non-focus genes were incorporated into the network until the size of the network elements reached 35 nodes. The core networks were ranked by score algorithmically based on their right-tailed Fisher's exact test *P*-value, which reflect the likelihood that the genes were grouped in a network by chance.

mRNA quantification by real-time RT–PCR

Total RNA in epididymal WAT was extracted by TRIzol followed with column purification with DNaseI treatment (Promega). In the case of hippocampus and hypothalamus, total RNA was extracted by using SV total RNA isolation system (Promega). Extracted total RNA was reverse transcribed with Super Script II (Life Technologies). Quantitative PCR (qPCR) was performed using SYBR Green real-time PCR system as described previously (73). *Actb* and *Gapdh* genes were used as internal controls for WAT and brain tissues, respectively. Primers sequences for qPCR are described in Table 4.

Generation of 3 Mb duplication mice using Cre/loxP chromosomal engineering system

Mice with transposon insertions between *Ndn* and *Ube3a* (lines 192 124 and 197 365)—TRACER database (74)—were isolated after *in vivo* remobilization of a transposon construct including a *loxP* site (34). The position on mouse chromosome 7 of the integrated *loxP* site was at 69 306 344 for 192 124 and 66 254 807 for 197 365, respectively (positions on NCBI37/*mm9* assembly). Duplication of the intervening segment [Dp (192 124–197 365)] was obtained by *in vivo* Cre-mediated recombineering in *trans* (75), with a *Hprt-Cre* transgene (76). From 61 animals screened by

Table 4. Primer sequences for RT–PCR

Primer name	Sequence (5′ to 3′)
Actb-F	CGTGCGTGACATCAAAGAGAA
Actb-R	TGGATGCCACAGGATTCCAT
Sfrp5-F	TGACCAAGATCTGTGCCCAGT
Sfrp5-R	TCAACTTTCGGTCCCCGTT
Gapdh-F	ACGGGAAGCTCACTGGCATGGCCTT
Gapdh-R	CATGAGGTCCACCACCCTGTTGCTG
Mkrn3-F	AGAGCATTCTGTGCTTCGCCT
Mkrn3-R	TACTGAAGCAAGAGCCAACGGT
Magel2-F	TTGGTGCCACTTTCTGTGCTC
Magel2-R	GGCAGGAAAGGTCTCTGATGTG
Ndn-F	GTATCCCAAATCCACAGTGC
Ndn-R	TAACTCTCCAGGGCCTTCTT
Snrpn-F	GCAAAACAGCCAGAACGTGAA
Snrpn-R	GCACACGAGCAATGCCAGTAT
Snord116-F	TGGATCTATGATGATTCCCAG
Snord116-R	TGGACCTCAGTTCCGATGAG
Snord115-F	GGGTCAATGATGACAACCCAATG
Snord115-R	GGGCCTCAGCGTAATCCTATTG
Ipw-F	TCACCACAACACTGGACAAAA
Ipw-R	TGCTGCTACACAGGAAAGAGG
Ube3a-ATS-F	GGCACCCTTGTTTGAAACTT
Ube3a-ATS-R	GCTCATGACCCTGTCCTTTC
Ube3a-F	TCTGCTGCTGCTATGGAAGA
Ube3a-R	CACATTCCACGTTAGGTGACA
Atp10a-F	CGCACTCACCATCTGCAATACA
Atp10a-R	CGTGAACCTCCGAAGGAAATCT
Gabrb3-F	GAATGTTGTCTTCGCCACAGGT
Gabrb3-R	ACCCACGAGAGGATTGTGATCA
Gabra5-F	TCCAAACATCCCAAAAGAGC
Gabra5-R	GAGAGGTGGCCCCTTTTATC
Gabrg3-F	CGAATAAGCCTTCAAGCACCC
Gabrg3-R	AGGTGTCCTCAAATTCCTGCC
Herc2-F	TGGCCCTTTAAGCCCCAAT
Herc2-R	GCCTATTAACCCCCAACCTATG

PCR, one *Dp*/+ animal was recovered as well as four mice carrying the reciprocal deletion *Df*/+ (192 124–197 365).

Copy number analysis by array comparative genomic hybridization

Array comparative genomic hybridization (aCGH) was performed according to the manufacturer's protocol (Agilent). Briefly, genomic DNA was extracted from tails of 3 Mb *patDp*/+ and WT mouse by DNeasy Blood & Tissue Kit (Qiagen) and aCGH was performed using Agilent's SurePrint G3 Mouse CGH Microarray Kit 1 × 1 M (G4838A, Agilent). Cy3 and Cy5 labeling and hybridization of genomic DNA was performed according to the manufacturer's instructions. DNA from a male WT mouse (C57BL/6J) was used as reference genomic DNA. The extracted signals were then analyzed under the R environment with DNAcopy, Gviz and GenomicRanges packages (77–79).

Open-field test

Locomotor activity of 3 Mb *patDp*/+ mice was measured by an open-field test. The experiment was conducted with 11- to 13-week-old mice. Each subject could move freely in the open-field apparatus (50 × 50 cm, O'Hara & Co.) illuminated at 100 lux (surface level of the arena). Horizontal locomotor activity was recorded for 30 min with a video camera and analyzed by OF software (O'Hara & Co.).

Statistical analysis

The data were expressed as mean values with their standard error unless noted otherwise. Analysis of mRNA expression levels is depicted as fold change compared with control. Data were analyzed with ANOVA and Tukey–Kramer *post-hoc* test was used for each significant difference. For other results, Student's *t*-test or the Mann–Whitney *U* test were used to compare WT and *patDp*/+ mice. The criterion for significance was set at $P < 0.05$.

Supplementary Material

Supplementary Material is available at *HMG* online.

Acknowledgements

We would like to thank T. Inagaki for suggestion of pair-fed experiment, Y. Watanabe for statistical consulting and all technical staffs of the Takumi Lab for technical assistance. We also thank A. Terashima for comments on the manuscript.

Funding

This work was supported in part by KAKENHI, Japan Society of Promotion of Science and Ministry of Education, Culture, Sports, Science and Technology, Strategic International Cooperative Program (SICP) and CREST, Japan Science and Technology Agency, Intramural Research Grant for Neurological and Psychiatric Disorders of NCNP, the Takeda Science Foundation and Takeda Pharmaceutical Co. Ltd.

References

1. Ogden, C.L., Carroll, M.D., Kit, B.K. and Flegal, K.M. (2014) Prevalence of childhood and adult obesity in the United States, 2011–2012. *JAMA*, **311**, 806–814.
2. Steppan, C.M., Bailey, S.T., Bhat, S., Brown, E.J., Banerjee, R.R., Wright, C.M., Patel, H.R., Ahima, R.S. and Lazar, M.A. (2001) The hormone resistin links obesity to diabetes. *Nature*, **409**, 307–312.
3. Haslam, D.W. and James, W.P. (2005) Obesity. *Lancet*, **366**, 1197–1209.
4. Adams, K.F., Schatzkin, A., Harris, T.B., Kipnis, V., Mouw, T., Ballard-Barbash, R., Hollenbeck, A. and Leitzmann, M.F. (2006) Overweight, obesity, and mortality in a large prospective cohort of persons 50 to 71 years old. *N. Engl. J. Med.*, **355**, 763–778.
5. Aguilera, C.M., Olza, J. and Gil, A. (2013) Genetic susceptibility to obesity and metabolic syndrome in childhood. *Nutr. Hosp.*, **28**(Suppl. 5), 44–55.
6. Robinson, S.W., Dinulescu, D.M. and Cone, R.D. (2000) Genetic models of obesity and energy balance in the mouse. *Annu. Rev. Genet.*, **34**, 687–745.
7. Cassidy, S.B., Schwartz, S., Miller, J.L. and Driscoll, D.J. (2012) Prader-Willi syndrome. *Genet. Med.*, **14**, 10–26.
8. Butler, M.G. (2011) Prader-Willi syndrome: obesity due to genomic imprinting. *Curr. Genomics*, **12**, 204–215.
9. Ohta, T., Gray, T.A., Rogan, P.K., Buiting, K., Gabriel, J.M., Saitoh, S., Muralidhar, B., Bilienska, B., Krajewska-Walasek, M., Driscoll, D.J. *et al.* (1999) Imprinting-mutation mechanisms in Prader-Willi syndrome. *Am. J. Hum. Genet.*, **64**, 397–413.
10. Mabb, A.M., Judson, M.C., Zylka, M.J. and Philpot, B.D. (2011) Angelman syndrome: insights into genomic imprinting and

neurodevelopmental phenotypes. *Trends Neurosci.*, **34**, 293–303.
11. Chamberlain, S.J. and Lalande, M. (2010) Angelman syndrome, a genomic imprinting disorder of the brain. *J Neurosci.*, **30**, 9958–9963.
12. Resnick, J.L., Nicholls, R.D. and Wevrick, R. and Prader-Willi Syndrome Animal Models Working, G. (2013) Recommendations for the investigation of animal models of Prader-Willi syndrome. *Mamm. Genome.*, **24**, 165–178.
13. Bervini, S. and Herzog, H. (2013) Mouse models of Prader-Willi syndrome: a systematic review. *Front. Neuroendocrinol.*, **34**, 107–119.
14. Hogart, A., Wu, D., LaSalle, J.M. and Schanen, N.C. (2010) The comorbidity of autism with the genomic disorders of chromosome 15q11.2-q13. *Neurobiol. Dis.*, **38**, 181–191.
15. Chamberlain, S.J. and Lalande, M. (2010) Neurodevelopmental disorders involving genomic imprinting at human chromosome 15q11-q13. *Neurobiol. Dis.*, **39**, 13–20.
16. Marini, C., Cecconi, A., Contini, E., Pantaleo, M., Metitieri, T., Guarducci, S., Giglio, S., Guerrini, R. and Genuardi, M. (2013) Clinical and genetic study of a family with a paternally inherited 15q11-q13 duplication. *Am. J. Med. Genet. A.*, **161A**, 1459–1464.
17. Engelen, J.J., Loots, W.J., Albrechts, J.C., Schrander-Stumpel, C.T., Dirckx, R., Smeets, H.J., Hamers, A.J. and Geraedts, J.P. (1999) Duplication within chromosome region 15q11-q13 in a patient with similarities to Prader-Willi syndrome confirmed by region-specific and band-specific fish. *Genet. Couns.*, **10**, 123–132.
18. Mao, R., Jalal, S.M., Snow, K., Michels, V.V., Szabo, S.M. and Babovic-Vuksanovic, D. (2000) Characteristics of two cases with dup(15)(q11.2-q12): one of maternal and one of paternal origin. *Genet. Med.*, **2**, 131–135.
19. Roberts, S.E., Dennis, N.R., Browne, C.E., Willatt, L., Woods, G., Cross, I., Jacobs, P.A. and Thomas, S. (2002) Characterisation of interstitial duplications and triplications of chromosome 15q11-q13. *Hum. Genet.*, **110**, 227–234.
20. Bolton, P.F., Dennis, N.R., Browne, C.E., Thomas, N.S., Veltman, M.W., Thompson, R.J. and Jacobs, P. (2001) The phenotypic manifestations of interstitial duplications of proximal 15q with special reference to the autistic spectrum disorders. *Am. J. Med. Genet.*, **105**, 675–685.
21. Veltman, M.W., Thompson, R.J., Craig, E.E., Dennis, N.R., Roberts, S.E., Moore, V., Brown, J.A. and Bolton, P.F. (2005) A paternally inherited duplication in the Prader-Willi/Angelman syndrome critical region: a case and family study. *J. Autism. Dev. Disord.*, **35**, 117–127.
22. Ungaro, P., Christian, S.L., Fantes, J.A., Mutirangura, A., Black, S., Reynolds, J., Malcolm, S., Dobyns, W.B. and Ledbetter, D.H. (2001) Molecular characterisation of four cases of intrachromosomal triplication of chromosome 15q11-q14. *J. Med. Genet.*, **38**, 26–34.
23. Nakatani, J., Tamada, K., Hatanaka, F., Ise, S., Ohta, H., Inoue, K., Tomonaga, S., Watanabe, Y., Chung, Y.J., Banerjee, R. *et al.* (2009) Abnormal behavior in a chromosome-engineered mouse model for human 15q11–13 duplication seen in autism. *Cell*, **137**, 1235–1246.
24. Tamada, K., Tomonaga, S., Hatanaka, F., Nakai, N., Takao, K., Miyakawa, T., Nakatani, J. and Takumi, T. (2010) Decreased exploratory activity in a mouse model of 15q duplication syndrome; implications for disturbance of serotonin signaling. *PLoS One*, **5**, e15126.
25. Takumi, T. (2011) The neurobiology of mouse models syntenic to human chromosome 15q. *J. Neurodev. Disord.*, **3**, 270–281.
26. Devalaraja-Narashimha, K. and Padanilam, B.J. (2010) PARP1 deficiency exacerbates diet-induced obesity in mice. *J. Endocrinol.*, **205**, 243–252.
27. Park, Y.J., Kim, S.C., Kim, J., Anakk, S., Lee, J.M., Tseng, H.T., Yechoor, V., Park, J., Choi, J.S., Jang, H.C. *et al.* (2011) Dissociation of diabetes and obesity in mice lacking orphan nuclear receptor small heterodimer partner. *J. Lipid. Res.*, **52**, 2234–2244.
28. Inagaki, T., Tachibana, M., Magoori, K., Kudo, H., Tanaka, T., Okamura, M., Naito, M., Kodama, T., Shinkai, Y. and Sakai, J. (2009) Obesity and metabolic syndrome in histone demethylase JHDM2a-deficient mice. *Genes Cells*, **14**, 991–1001.
29. Miller, J.L., Lynn, C.H., Driscoll, D.C., Goldstone, A.P., Gold, J.A., Kimonis, V., Dykens, E., Butler, M.G., Shuster, J.J. and Driscoll, D.J. (2011) Nutritional phases in Prader-Willi syndrome. *Am. J. Med. Genet. A.*, **155A**, 1040–1049.
30. Galarraga, M., Campion, J., Munoz-Barrutia, A., Boque, N., Moreno, H., Martinez, J.A., Milagro, F. and Ortiz-de-Solorzano, C. (2012) Adiposoft: automated software for the analysis of white adipose tissue cellularity in histological sections. *J. Lipid. Res.*, **53**, 2791–2796.
31. Lv, C., Jiang, Y., Wang, H. and Chen, B. (2012) Sfrp5 expression and secretion in adipocytes are up-regulated during differentiation and are negatively correlated with insulin resistance. *Cell. Biol. Int.*, **36**, 851–855.
32. Koza, R.A., Nikonova, L., Hogan, J., Rim, J.S., Mendoza, T., Faulk, C., Skaf, J. and Kozak, L.P. (2006) Changes in gene expression foreshadow diet-induced obesity in genetically identical mice. *PLoS Genet.*, **2**, e81.
33. Mori, H., Prestwich, T.C., Reid, M.A., Longo, K.A., Gerin, I., Cawthorn, W.P., Susulic, V.S., Krishnan, V., Greenfield, A. and Macdougald, O.A. (2012) Secreted frizzled-related protein 5 suppresses adipocyte mitochondrial metabolism through WNT inhibition. *J. Clin. Invest.*, **122**, 2405–2416.
34. Ruf, S., Symmons, O., Uslu, V.V., Dolle, D., Hot, C., Ettwiller, L. and Spitz, F. (2011) Large-scale analysis of the regulatory architecture of the mouse genome with a transposon-associated sensor. *Nat. Genet.*, **43**, 379–386.
35. Jiang, Y.H., Armstrong, D., Albrecht, U., Atkins, C.M., Noebels, J.L., Eichele, G., Sweatt, J.D. and Beaudet, A.L. (1998) Mutation of the Angelman ubiquitin ligase in mice causes increased cytoplasmic p53 and deficits of contextual learning and long-term potentiation. *Neuron*, **21**, 799–811.
36. Gustin, R.M., Bichell, T.J., Bubser, M., Daily, J., Filonova, I., Mrelashvili, D., Deutch, A.Y., Colbran, R.J., Weeber, E.J. and Haas, K.F. (2010) Tissue-specific variation of Ube3a protein expression in rodents and in a mouse model of Angelman syndrome. *Neurobiol. Dis.*, **39**, 283–291.
37. Judson, M.C., Sosa-Pagan, J.O., Del Cid, W.A., Han, J.E. and Philpot, B.D. (2014) Allelic specificity of Ube3a expression in the mouse brain during postnatal development. *J. Comp. Neurol.*, **522**, 1874–1896.
38. Albrecht, U., Sutcliffe, J.S., Cattanach, B.M., Beechey, C.V., Armstrong, D., Eichele, G. and Beaudet, A.L. (1997) Imprinted expression of the murine Angelman syndrome gene, Ube3a, in hippocampal and Purkinje neurons. *Nat. Genet.*, **17**, 75–78.
39. Depienne, C., Moreno-De-Luca, D., Heron, D., Bouteiller, D., Gennetier, A., Delorme, R., Chaste, P., Siffroi, J.P., Chantot-Bastaraud, S., Benyahia, B. *et al.* (2009) Screening for genomic rearrangements and methylation abnormalities of the 15q11-q13 region in autism spectrum disorders. *Biol. Psychiatry*, **66**, 349–359.
40. Dimitropoulos, A. and Schultz, R.T. (2007) Autistic-like symptomatology in Prader-Willi syndrome: a review of recent findings. *Curr. Psychiatry. Rep.*, **9**, 159–164.

41. Bruining, H., Eijkemans, M.J., Kas, M.J., Curran, S.R., Vorstman, J.A. and Bolton, P.F. (2014) Behavioral signatures related to genetic disorders in autism. *Mol. Autism.*, **5**, 11.
42. Schaaf, C.P., Gonzalez-Garay, M.L., Xia, F., Potocki, L., Gripp, K.W., Zhang, B., Peters, B.A., McElwain, M.A., Drmanac, R., Beaudet, A.L. *et al.* (2013) Truncating mutations of MAGEL2 cause Prader-Willi phenotypes and autism. *Nat. Genet.*, **45**, 1405–1408.
43. Gallagher, R.C., Pils, B., Albalwi, M. and Francke, U. (2002) Evidence for the role of PWCR1/HBII-85 C/D box small nucleolar RNAs in Prader-Willi syndrome. *Am. J. Hum. Genet.*, **71**, 669–678.
44. Schule, B., Albalwi, M., Northrop, E., Francis, D.I., Rowell, M., Slater, H.R., Gardner, R.J. and Francke, U. (2005) Molecular breakpoint cloning and gene expression studies of a novel translocation t(4;15)(q27;q11.2) associated with Prader-Willi syndrome. *BMC Med. Genet.*, **6**, 18.
45. de Smith, A.J., Purmann, C., Walters, R.G., Ellis, R.J., Holder, S.E., Van Haelst, M.M., Brady, A.F., Fairbrother, U.L., Dattani, M., Keogh, J.M. *et al.* (2009) A deletion of the HBII-85 class of small nucleolar RNAs (snoRNAs) is associated with hyperphagia, obesity and hypogonadism. *Hum. Mol. Genet.*, **18**, 3257–3265.
46. Duker, A.L., Ballif, B.C., Bawle, E.V., Person, R.E., Mahadevan, S., Alliman, S., Thompson, R., Traylor, R., Bejjani, B.A., Shaffer, L.G. *et al.* (2010) Paternally inherited microdeletion at 15q11.2 confirms a significant role for the SNORD116 C/D box snoRNA cluster in Prader-Willi syndrome. *Eur. J. Hum. Genet.*, **18**, 1196–1201.
47. Sahoo, T., del Gaudio, D., German, J.R., Shinawi, M., Peters, S. U., Person, R.E., Garnica, A., Cheung, S.W. and Beaudet, A.L. (2008) Prader-Willi phenotype caused by paternal deficiency for the HBII-85 C/D box small nucleolar RNA cluster. *Nat. Genet.*, **40**, 719–721.
48. Skryabin, B.V., Gubar, L.V., Seeger, B., Pfeiffer, J., Handel, S., Robeck, T., Karpova, E., Rozhdestvensky, T.S. and Brosius, J. (2007) Deletion of the MBII-85 snoRNA gene cluster in mice results in postnatal growth retardation. *PLoS Genet.*, **3**, e235.
49. Ding, F., Li, H.H., Zhang, S., Solomon, N.M., Camper, S.A., Cohen, P. and Francke, U. (2008) SnoRNA Snord116 (Pwcr1/MBII-85) deletion causes growth deficiency and hyperphagia in mice. *PLoS One*, **3**, e1709.
50. Ding, F., Li, H.H., Li, J., Myers, R.M. and Francke, U. (2010) Neonatal maternal deprivation response and developmental changes in gene expression revealed by hypothalamic gene expression profiling in mice. *PLoS One*, **5**, e9402.
51. Powell, W.T., Coulson, R.L., Crary, F.K., Wong, S.S., Ach, R.A., Tsang, P., Alice Yamada, N., Yasui, D.H. and Lasalle, J.M. (2013) A Prader-Willi locus lncRNA cloud modulates diurnal genes and energy expenditure. *Hum. Mol. Genet.*, **22**, 4318–4328.
52. Lin, D., Wang, Q., Ran, H., Liu, K., Wang, Y., Wang, J., Liu, Y., Chen, R., Sun, Y., Liu, R. *et al.* (2014) Abnormal response to the anorexic effect of GHS-R inhibitors and exenatide in male Snord116 deletion mouse model for Prader-Willi syndrome. *Endocrinology*, **155**, 2355–2362.
53. Goldstone, A.P., Thomas, E.L., Brynes, A.E., Bell, J.D., Frost, G., Saeed, N., Hajnal, J.V., Howard, J.K., Holland, A. and Bloom, S.R. (2001) Visceral adipose tissue and metabolic complications of obesity are reduced in Prader-Willi syndrome female adults: evidence for novel influences on body fat distribution. *J. Clin. Endocrinol. Metab.*, **86**, 4330–4338.
54. Kishore, S. and Stamm, S. (2006) The snoRNA HBII-52 regulates alternative splicing of the serotonin receptor 2C. *Science*, **311**, 230–232.
55. Doe, C.M., Relkovic, D., Garfield, A.S., Dalley, J.W., Theobald, D.E., Humby, T., Wilkinson, L.S. and Isles, A.R. (2009) Loss of the imprinted snoRNA mbii-52 leads to increased 5htr2c pre-RNA editing and altered 5HT2CR-mediated behaviour. *Hum. Mol. Genet.*, **18**, 2140–2148.
56. Ding, F., Prints, Y., Dhar, M.S., Johnson, D.K., Garnacho-Montero, C., Nicholls, R.D. and Francke, U. (2005) Lack of Pwcr1/MBII-85 snoRNA is critical for neonatal lethality in Prader-Willi syndrome mouse models. *Mamm. Genome.*, **16**, 424–431.
57. Vitali, P., Basyuk, E., Le Meur, E., Bertrand, E., Muscatelli, F., Cavaille, J. and Huttenhofer, A. (2005) ADAR2-mediated editing of RNA substrates in the nucleolus is inhibited by C/D small nucleolar RNAs. *J. Cell. Biol.*, **169**, 745–753.
58. Burns, C.M., Chu, H., Rueter, S.M., Hutchinson, L.K., Canton, H., Sanders-Bush, E. and Emeson, R.B. (1997) Regulation of serotonin-2C receptor G-protein coupling by RNA editing. *Nature*, **387**, 303–308.
59. Flomen, R., Knight, J., Sham, P., Kerwin, R. and Makoff, A. (2004) Evidence that RNA editing modulates splice site selection in the 5-HT2C receptor gene. *Nucleic Acids Res.*, **32**, 2113–2122.
60. Tecott, L.H., Sun, L.M., Akana, S.F., Strack, A.M., Lowenstein, D.H., Dallman, M.F. and Julius, D. (1995) Eating disorder and epilepsy in mice lacking 5-HT2c serotonin receptors. *Nature*, **374**, 542–546.
61. Kawahara, Y., Grimberg, A., Teegarden, S., Mombereau, C., Liu, S., Bale, T.L., Blendy, J.A. and Nishikura, K. (2008) Dysregulated editing of serotonin 2C receptor mRNAs results in energy dissipation and loss of fat mass. *J. Neurosci.*, **28**, 12834–12844.
62. Johnstone, K.A., DuBose, A.J., Futtner, C.R., Elmore, M.D., Brannan, C.I. and Resnick, J.L. (2006) A human imprinting centre demonstrates conserved acquisition but diverged maintenance of imprinting in a mouse model for Angelman syndrome imprinting defects. *Hum. Mol. Genet.*, **15**, 393–404.
63. Huang, H.S., Burns, A.J., Nonneman, R.J., Baker, L.K., Riddick, N.V., Nikolova, V.D., Riday, T.T., Yashiro, K., Philpot, B.D. and Moy, S.S. (2013) Behavioral deficits in an Angelman syndrome model: effects of genetic background and age. *Behav. Brain Res.*, **243**, 79–90.
64. Meng, L., Ward, A.J., Chun, S., Bennett, C.F., Beaudet, A.L. and Rigo, F. (2015) Towards a therapy for Angelman syndrome by targeting a long non-coding RNA. *Nature*, **518**, 409–412.
65. Brennan, M.L., Adam, M.P., Seaver, L.H., Myers, A., Schelley, S., Zadeh, N., Hudgins, L. and Bernstein, J.A. (2015) Increased body mass in infancy and early toddlerhood in Angelman syndrome patients with uniparental disomy and imprinting center defects. *Am. J. Med. Genet. A.*, **167A**, 142–146.
66. Ross, S.E., Hemati, N., Longo, K.A., Bennett, C.N., Lucas, P.C., Erickson, R.L. and MacDougald, O.A. (2000) Inhibition of adipogenesis by Wnt signaling. *Science*, **289**, 950–953.
67. Bennett, C.N., Ross, S.E., Longo, K.A., Bajnok, L., Hemati, N., Johnson, K.W., Harrison, S.D. and MacDougald, O.A. (2002) Regulation of Wnt signaling during adipogenesis. *J. Biol. Chem.*, **277**, 30998–31004.
68. Cavaille, J., Buiting, K., Kiefmann, M., Lalande, M., Brannan, C.I., Horsthemke, B., Bachellerie, J.P., Brosius, J. and Huttenhofer, A. (2000) Identification of brain-specific and imprinted small nucleolar RNA genes exhibiting an unusual genomic organization. *Proc. Natl Acad. Sci. USA*, **97**, 14311–14316.

69. Rogelj, B., Hartmann, C.E., Yeo, C.H., Hunt, S.P. and Giese, K.P. (2003) Contextual fear conditioning regulates the expression of brain-specific small nucleolar RNAs in hippocampus. *Eur. J. Neurosci.*, **18**, 3089–3096.
70. Yang, T., Adamson, T.E., Resnick, J.L., Leff, S., Wevrick, R., Francke, U., Jenkins, N.A., Copeland, N.G. and Brannan, C.I. (1998) A mouse model for Prader-Willi syndrome imprinting-centre mutations. *Nat. Genet.*, **19**, 25–31.
71. Gentleman, R., Carey, V., Huber, W., Irizarry, R. and Dudoit, S. (2005) *Bioinformatics and Computational Biology Solutions Using R and Bioconductor*, Springer, New York.
72. Smyth, G.K. (2004) Linear models and empirical Bayes methods for assessing differential expression in microarray experiments. *Stat. Appl. Genet. Mol. Biol.*, **3**, Article 3.
73. Akashi, M. and Takumi, T. (2005) The orphan nuclear receptor RORalpha regulates circadian transcription of the mammalian core-clock Bmal1. *Nat. Struct. Mol. Biol.*, **12**, 441–448.
74. Chen, C.K., Symmons, O., Uslu, V.V., Tsujimura, T., Ruf, S., Smedley, D. and Spitz, F. (2013) TRACER: a resource to study the regulatory architecture of the mouse genome. *BMC Genomics*, **14**, 215.
75. Herault, Y., Rassoulzadegan, M., Cuzin, F. and Duboule, D. (1998) Engineering chromosomes in mice through targeted meiotic recombination (TAMERE). *Nat. Genet.*, **20**, 381–384.
76. Tang, S.H., Silva, F.J., Tsark, W.M. and Mann, J.R. (2002) A Cre/loxP-deleter transgenic line in mouse strain 129S1/SvImJ. *Genesis*, **32**, 199–202.
77. Seshan, V.E. and Olshen, A. DNAcopy: DNA copy number data analysis. R package version 1.40.0.
78. Hahne, F., Durinck, S., Ivanek, R., Mueller, A., Lianoglou, S., Tan, G. and Parsons, L. Gviz: plotting data and annotation information along genomic coordinates. R package version 1.10.10.
79. Lawrence, M., Huber, W., Pages, H., Aboyoun, P., Carlson, M., Gentleman, R., Morgan, M.T. and Carey, V.J. (2013) Software for computing and annotating genomic ranges. *PLoS Comput. Biol.*, **9**, e1003118.